JLAB12 Activity report 2019

V. Lucherini, M. Mirazita (Resp.), D. Orecchini(Tecn.), A. Orlandi(Tecn.),
C. Pecar (DOE-INFN Summer Students fellowship), P. Rossi,
O. Soto (INFN fellowship), S. Tomassini

1 Introduction

The JLAB12 group of LNF participates in the physics program carried on by the CLAS collaboration in the Hall B of the Jefferson Laboratory (JLab). The LNF group has been deeply involved in the data taking and in the first analyses of the physics data. The overall performance of the CLAS12 spectometer and of its subsystems, including the RICH, has been carefully studied and a number of review papers to report the results is in print by the NIM journal.

In parallel, the construction of the second RICH module has been started.

2 The CLAS12 RICH

The detector is composed by an aerogel radiator, an array of multianode photomultiplier tubes (MAPMTs) for the Cherenkov light detection and a mirror system. All these elements are contained in a large trapezoidal box, of approximate height of 3.5 m and large base of about 4 m.

The radiator is composed by tiles with squared shape 20×20 cm^2 as well as smaller pentagonal, trapezoidal or triangular tiles to accomodate with the detector shape. The total number of tiles is 102, assembled in two sections: the forward angle one made by one layer with 2 cm thickness and the large angle one made by two layers with 3 cm thickness each.

The mirror system is composed by 10 carbon fiber spherical mirrors and 7 glass planar mirros, for a total surface of about 10 m^2. The goal of the mirror system is to contain as much of the produced Cherenkov inside the detector and to direct them toward the photodetector array.

The photodector array uses 391 MAPMT Hamamatsu H8500 and H12700. These two types of tubes are composed by a matrix of 8×8 matrix of pixel with about 6 mm pixel size, with a total of 25024 independent readout channels.

The readout electronics is based on the MAROC3 chip, a 64 channel microcircuit dedicated to MAPMT pulse processing. Each channel offers a low impedence adjustable gain preamplifier followed by a highly configurable shaping section, and produces both prompt logic pulses from an adjustable threshold discriminator. The MAROC is configured and read out by a FPGA optically linked with the data acquisition node. The front-end electronics is organized in compact units mechanically designed to fit the MAPMT dimensions and serving two or three MAPMTs each, thus allowing the tessellation of large surfaces with minimum dead space and material budget.

2.1 Study of the performance of the RICH

The PID in the RICH is based on a likelihood approach, in which the measured photon hit pattern is compared to the expected one based on the charged tracks entering in the detector. This likelihood approach requires the precise mapping of the timing and Cherenkov angle resolutions.

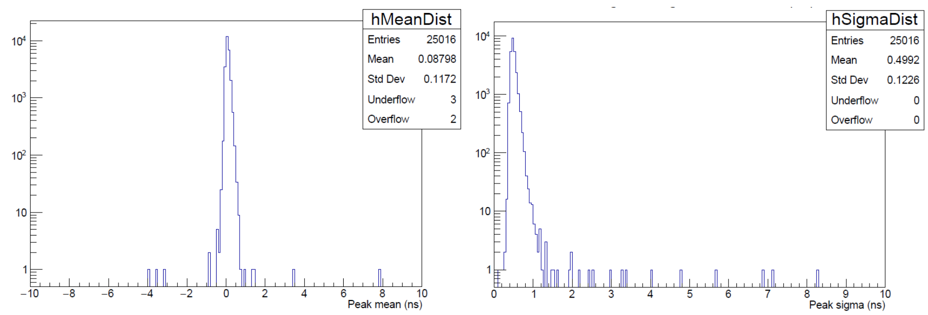

Figure 1: *Typical dstributions of the mean (left plot) and σ (right plot) of the ΔT distributions for all the readout channels.*

2.1.1 Timing performance

The RICH timing performance is studied by using electrons and charged pions identified in the CLAS12 with momentum bigger than 1.5 GeV/c. The basic quantities for this study is the time difference

$$\Delta T = T_{meas} - T_{calc} \tag{1}$$

where T_{meas} is the measured time of the photon hit, after time offset and time walk corrections have been applied, while T_{calc} is the expected hit time, based on the known path of the charged track from the production vertex to the aerogel radiator and the recostructed photon path inside the RICH. The latter is computed in the RICH reconstruction software knowing the geometry of the detector and taking into account all the possible reflections on the planar and spherical mirrors.

The distribution of the ΔT is plotted for each one of the 25024 readout channels, it is fitted with a gaussian curve and the mean and the σ of the fits are extracted. In Fig. 1, we show an example of the obtained results. The left plot shows the distribution of all the gaussian means, which are center to zero with an RMS of the order of 100 ps. The left plot shows the σ s, which have an average value of 0.5 ns with an RMS of about 100 ps. The few channels with mean away from zero or larger σ are typically channels with low statistics where a reliable gaussian fit cannot be performed.

The timing parameters are periodically checked during the data taking and the obtained values are stored in the CLAS database.

2.1.2 Cherenkov angle reconstruction performance

Given a photon hit on the MAPMT plane and a charged track crossing the aerogel radiator, the emission angle is reconstructed using a ray tracing approach and the known geometry of the active elements of the detector. Each aerogel tile presents specific features because the challenging production process, tuned to achieve the highest transparency over a large volume, is not fully industrialized. Therefore, a detailed mapping of the refractive index across the surface of each tile is extracted from the experimental data. To this goal, high energy electrons, producing Cherenkov photons with saturated angle, are used and various detection topologies have been identified, namely:

- photons detected by the MAPMTs without any reflection (direct photons);
- photons with first reflection on one of the planar mirrors;
- photons with first reflection on one of the spherical mirrors.

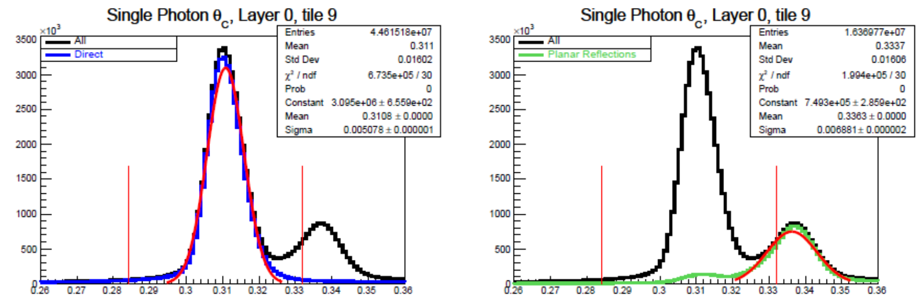

Figure 2: *Cherenkov angle distributions for photons emitted by tile 9 in layer 0. Left plot: all photons (black histogram) and direct photons (blue histogram). Right plot: all photons (black histogram) and photons with first reflection on the planar mirrors (green histogram).*

The reflected photons can be further classified according to the number of reflections. A preliminary study of the RICH performance has been carried out using about 10% of the collected data.

In Fig. 2, we show the Cherenkov angle distributions for the tile number 9 in the first sector of 2 cm thickness aerogel (layer 0). In the two plots, the black histograms show all the photons. The blue histogram on the left plots represents the direct photons, while the green histogram on the right represents the planar reflection photons. We see that the direct photons exhibit a narrow peak, with a resolution of about 4.5 mrad. For the reflected photons, we see a main peak with single reflection on one of the lateral mirrors, shifted to larger Cherenkov angle because of the misalignment of the mirror has not been corrected yet. We also see a weaker peak at smaller angles due to photons with multiple reflections. No photons with reflection on the spherical mirrors for this aerogel tile have been detected.

Thanks to the precise reconstruction of the impact point of the charged track, the tile surface has been divided in a finer 7×7 grid, each quadrant of the grid having a side length of about 3 cm. The results for the tile 9 in layer 0 are shown in the Fig. 3. The direct photon distributions have been fitted with a gaussian curve to extract mean and sigma of the Cherenkov angle. In this way, a precise mapping of the Cherenkov angle mean and resolution has been extrected from the data.

The Fig. 4 shows a pictorial representation of the results obtained for the two sectors of 2 cm thickness tiles. Each square in the plots represent an aerogel tile, which is further divided in the matrix of 7×7 pixels. The values of the Cherenkov angle means (left plot) can vary from tile to tile up to few mrad, however the variations across the tile surface are much smaller. The measured resolutions (right plot) are of the order of 4.5 mrad across basically the whole two layers, which is very close to the specification design to achieve a 4σ separation between kaons and pions. Higher resolutions for few edge pixels in the map are due to the limited statistics that doesn't allow a reliable fit.

This study will be further improved once the whole set of the collected data will be available. The higher statistics will allow a finer pixelization of the aerogel surface and will allow the study of the photons reflected on the spherical mirrors. Once completed, the results of this study will be uploaded on the CLAS12 database and will be input parameters for the likelihood function that will be used in the particle identification algorithm.

2.1.3 First look at the PID performance

A first look at the RICH particle identification response can be obtained by plotting the average Cherenkov angle per charged track as a function of the track momentum. This plot is shown in

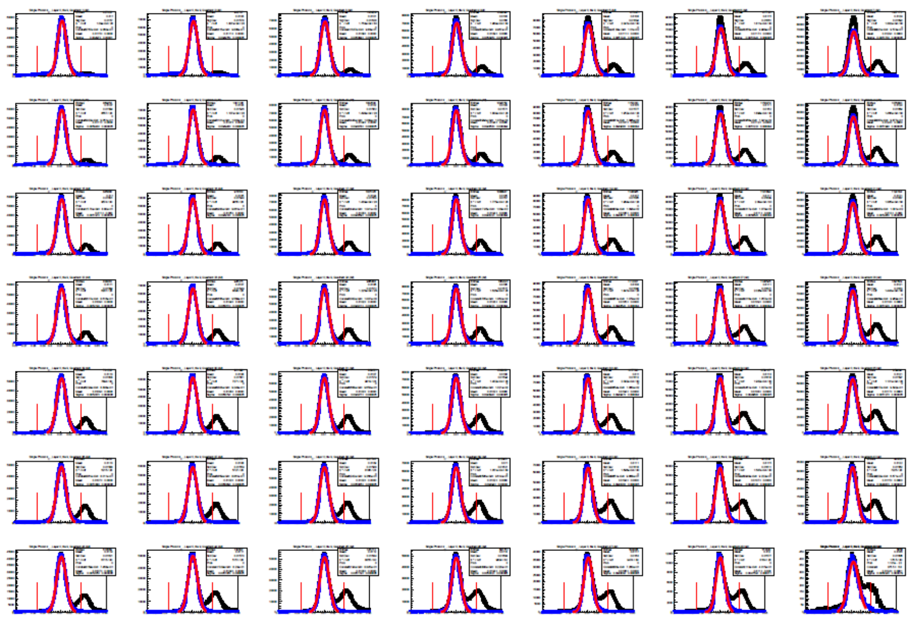

Figure 3: *Cherenkov angle distributions for photons emitted by tile 9 in layer 0, in a grid of* 7×7 *quadrants: all photons (black histograms) and direct photons (blue histograms).*

Fig. 5 for positively charged tracks.

Although many reconstruction parameters still have to be optimized, we can clearly see the three separated bands corresponding to π^+, K^+ and protons. Here, a fiducial Cherenkov angle region based on the expected resolutions has been defined in order to accept or reject reconstructed photons in the track average. As a result, a substantial fraction of the photons reflected by misaligned mirrors has been rejected (see for example the right plot in Fig. 2). We expect that these photons will be recovered once the alignment procedure will be completed, with a significant improvement in the separation power.

2.2 Construction of the second RICH module

The installation of a second RICH module is planned, allowing to double the charged kaon acceptance of the CLAS12 spectrometer and also to better control the systematics uncertainties in the future measurements with polarized targets.

The contruction of the second module, with the same geometry of the first one, is currently underway under the supervision of the physicists, technologits and technicians of the LNF group. The construction of the mechanical structure of the detector has been awarded in 2018 to the same that built the first module, and is currently underway. The purchase of the internal components is also underway. The orders for the purchase of the aerogel radiator, for a first bunch of 121 MAPMTs and for the planar mirrors have been placed and their production has started. The installation of the second module in CLAS12 is foreseen for the summer 2021.

3 Physics data analysis

The LNF groups is involved in data analysis aiming at the study of the internal structure of the nucleon through the measurements of Semi-Inclusive Deep Inelastic Scattering (SIDIS) of polarized

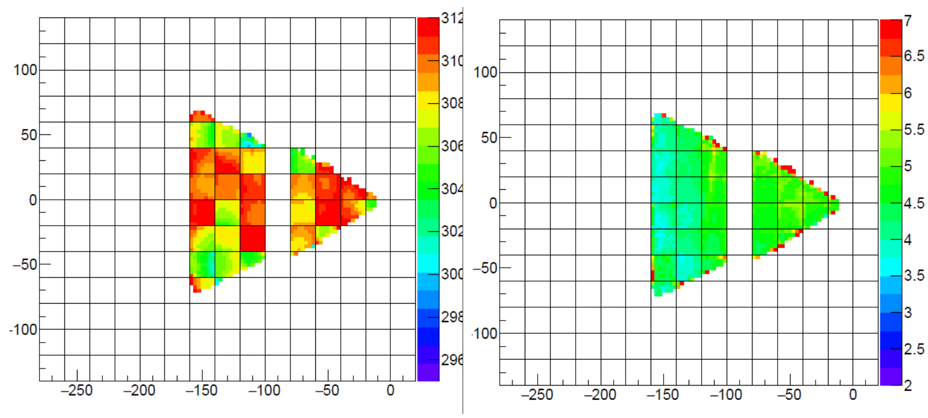

Figure 4: *Pictorial maps of the Cherenkov angle mean (left) and width (right) measured with electrons. Each square represent a tile, which is further divided in a matrix of* 7×7 *pixels. The color scale is mrad. Results for the two aerogel layer of 2 cm thickness tiles.*

electrons on a fixed target and looking at final states with one or more hadron. The underlying reaction mechanism can be schematized with a virtual photon exchanged by the incoming electron and the target that interacts with one of the quark composing the nucleon. After the interaction, the struck quark fragments into the observed hadron(s). The presence of the final hadrons allows the access to a number of spin-orbit correlations between the transverse momentum and the spin of the quarks with the transverse momentum of the hadron. The relevant quantities in these measurements are the Transverse Momentum Dependent (TMD) functions, 3-dimensional extensions of the well known collinear Partonic Distribution Functions (PDFs).

3.1 Di-hadron SIDIS electroproduction

The SIDIS cross section can be expanded in a series of harmonics in th azimuthal angles of the final hadrons. The coefficients of the azimuthal angle modulations are the structure functions F_{IJ} where the two subscripts indicate unpolarized (U), longitudinally (L) or transversely (T) polarized beam or target nucleon. These structure functions are in turn convolution of one TMD and one Fragmentation Function (FF), describing the fragmentation of the struck quark into the final hadrons.

A particularly interesting reaction channel is the SIDIS two-pion electroproduction channel. In fact, the presence of two hadrons in the final state allows tha access to spin orbit correlations even in the collinear limit (i.e. by integrating over the transverse momentum of the hadron pair), leading to a simpler interpretation of the results.

Analysis of the dihadron SIDIS electroproduction are underway with both old CLAS 6 GeV data and new CLAS12 data at 12 GeV.

3.2 Di-hadron SIDIS with CLAS data at 6 GeV

The experimental data have been collected back in 2003 within the *e1f* experiment. The electron beam with 5.5 GeV energy and 75% polarization was sent to a liquid hydrogen target. The scattered electron and the two opposite charge pions were detected in CLAS. A total of about 60k $e\pi^+\pi^-X$ events has been collected.

The measured observable is the Beam Spin Asymmetry (BSA), defined (up to some kinematic

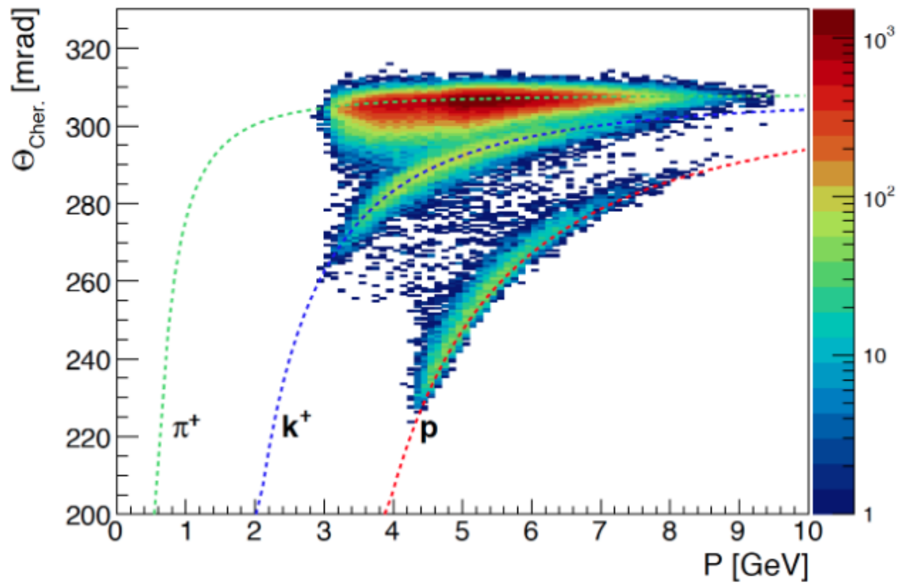

Figure 5: *Average Cherenkov angle per track as a function of the momentum for positively charged tracks in the RICH. The dashed lines represent the expected curves for π^+, K^+ and protons.*

factor) as the ratio:

$$BSA \propto \frac{F_{LU}}{F_{UU}} \sin\phi = A_{LU}^{\sin\phi} \sin\phi \tag{2}$$

Experimentally, the BSA can be written as

$$BSA = \frac{1}{P_B} \frac{N^+ - N^-}{N^+ + N^-} \tag{3}$$

where $N^{\pm}$ are the number events with positive or negative electron helicity and P_B is the average beam polarization. The $\sin\phi$ moment of the BSA is then extracted by fitting the measured BSA with eq. (2). The results as a function of the Bjorken-x variable x_B, the fractional energy of the pion pair z and of their invariant mass M_h are shown in Fig. 6. The signal is signficantly non-zero at the smaller x_B bin, then decreases as x_B increases and is consistent with zero within 1σ in the last x_B bin. The z and M_h dependencies show a small signal, which is at best about 1σ above zero.

The analysis is now under review by the CLAS Collaboration.

3.3 Di-hadron SIDIS with CLAS12 data at 12 GeV

A similar analysis is underway on the data taken in 2018 and 2019 with the CLAS12 spectrometer, in which a 10.6 GeV electron beam energy with polarization larger than 80% was sent to an unpolarized target of liquid hydrogen and deuterium. The luminosity of 10^{35} cm^{-2} s^{-1} will allow to study the reaction with unprecedented statistical precision. In addition, the two targets will allow the separation of the contributions of the quarks u and d to the measured asymmetries.

A first sample of about 10% of the collected hydrogen data has been prepared in 2019, in order to verify the CLAS12 performance and to define the particle identification cut. Preliminary

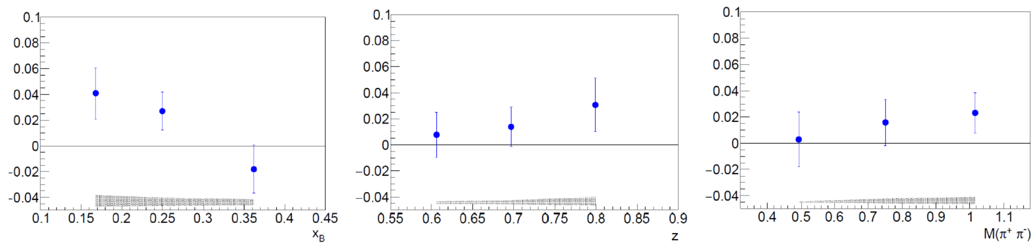

Figure 6: *The* $\sin\phi$ *moment of the BSA measured in CLAS as a function of* x_B *(left),* z *(center) and* $M-h$ *(right).*

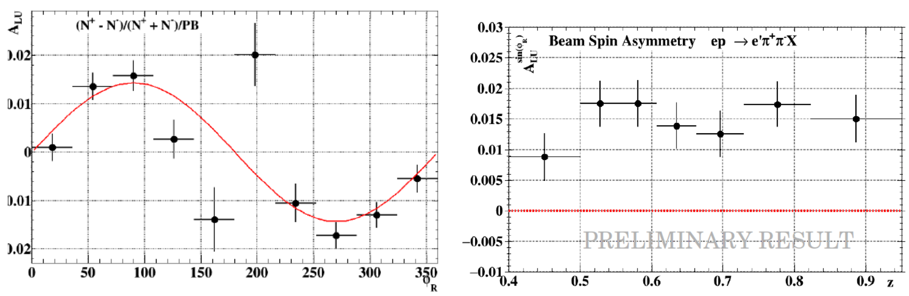

Figure 7: *The* ϕ *dependence of the BSA measured in CLAS12 integrated over the whole kinematics (left plot) and the* z *dependence of the moment* $A_{LU}^{\sin\phi}$ *(right plot).*

results of the analysis with this small sample have been presented at the 105^{th} National Congress of the Italian Physics Society. The left plot in the Fig. 7 we shows the ϕ dependence of the BSA integrated over the whole kinematic plane, with the fit to extract the moment $A_{LU}^{\sin\phi}$. The right plot of the figure shows the z dependence of the moment. A signal of the order of 2% is measured, with a statistical precision much better than the one measure dwith CLAS already with the limited data sample used here.

The CLAS Collaboration is now working on the production of the entire data collected with both targets.

4 Publications

Main publications.

1. The CLAS Collaboration, "The CLAS12 spectrometer", dedicated volume of Nucl. Inst. Meth., in print.

2. M. Mirazita, P. Rossi, V. Lucherini, D. Orecchini, C. Pecar, S. Tomassini *et al.*, "The CLAS12 Ring Imaging Cherenkov Detector", Nucl. Inst. Meth., in print.

3. M. Mirazita *et al.*, "The CLAS12 Geant4 Simulation", Nucl. Inst. Meth., in print.